

## Electron Impact Detachment of Weakly Bound Negative Ions

F. Robicieux

*Department of Physics, 206 Allison Laboratory, Auburn University, Auburn, Alabama 36849-5311*

(Received 1 June 1998)

A method is presented for accurately calculating the total electron impact detachment cross section for weakly bound negative ions. The results are compared to recent experiments for electron impact detachment of  $H^-$  and  $B^-$ . Cross sections differential in energy are presented which elucidate some of the dynamics of the detachment process. A scaling law for the cross section is proposed. [S0031-9007(98)08313-6]

PACS numbers: 34.80.Kw, 34.10.+x

There have been several recent experiments measuring the electron impact detachment of atomic and molecular negative ions [1–8]. These experiments exemplify one of the more important processes in physics: the breaking of a target by a projectile giving at least three distinct bodies in the final state. This process is especially difficult to describe theoretically due to the necessity for describing two continua. In this paper, I describe an accurate method for calculating cross sections that takes advantage of the nature of the double continua for electron detachment of negative ions. The calculated cross sections have been dissected in order to gain an understanding of the dynamics governing the detachment process. The insight thus obtained leads to scaling rules for detachment from weakly bound negative ions (ions for which the weakly bound electron is most likely found outside of the region that contains the atomic electrons).

There have been four previous methods used to describe electron impact detachment of negative ions. A brief description of these calculations may give some insight into the difficulties that must be overcome. The first method [9] used what is now called an  $R$ -matrix pseudostate method to calculate the detachment as an excitation to a positive energy pseudostate. This method did not achieve converged cross sections due to the slow decrease of cross section with increasing total angular momentum. The second method [5] utilized a classical, phenomenological technique. The total detachment cross section is estimated to be the cross section for a classical electron moving in a repulsive Coulomb potential to be absorbed by a partially absorbing sphere of radius  $r_0$ . This radius and the absorbing fraction are fitted to the experimentally measured detachment cross section.

The third method [10] used a fully quantum first order distorted wave theory. Electron wave functions separable in  $\vec{r}_1$  and  $\vec{r}_2$  (the two outgoing electron's coordinates) are used for both the initial and the final states. The initial state is nearly separable in  $\vec{r}_1$  and  $\vec{r}_2$  since it describes one electron weakly bound to the atom/molecule and the projectile electron in a continuum state. However, the final state is not expected to be separable in these coordinates since the final state wave function describes two highly correlated electrons that are both in the continuum. The

method is somewhat sensitive to the potential in which the electron waves are calculated, but the theoretical cross sections are in qualitative agreement with experiment. The fourth method [11–13] is a semiquantum technique in which the electron that is attached to the atom is treated quantum mechanically while the projectile electron is treated as a classical particle. The trajectory of the “classical electron” is a hyperbola that arises when a charged particle of incident energy  $E_i$  interacts with an infinitely massive object of the same charge. It is not possible to include electron exchange in this method nor is it possible to make successive improvements on the main approximation (a classical electron projectile). Even within the classical electron approximation, there is a difficulty in correctly describing the final state dynamics since the projectile electron does not change its energy and does not respond to changes in the negative ion target state during the collision process. This method gives surprisingly good agreement with experiment for the  $e^- + H^- \rightarrow H + 2e^-$  total cross section but the uncertainties in this method make it difficult to estimate how accurate the method should be in different energy ranges and for different negative ions.

All of the theoretical methods described above utilize radically different approximations in the attempt to account for the dynamics of a double electron continuum. A completely different method for treating the double electron continuum is presented in this paper. This method should be more accurate than previous methods and should give quantitatively accurate total and differential cross sections thus providing some insight into the details of the dynamics. In principle, the method can be improved if needed.

The basic approximation and insight into the dynamics may be obtained from a two electron Hamiltonian in which each of the electrons interact with an infinitely heavy atom through a short-range potential  $U(r)$ . The Hamiltonian in the  $\vec{r}_1, \vec{r}_2$  coordinate system is

$$H = -\frac{1}{2} \nabla_1^2 - \frac{1}{2} \nabla_2^2 + U(r_1) + U(r_2) + 1/|\vec{r}_2 - \vec{r}_1|. \quad (1)$$

This clearly shows the difficulty in using this coordinate system to describe the final state since the  $1/|\vec{r}_2 - \vec{r}_1|$  potential causes correlation between the two electrons out to enormous distances. However, this correlation is an artifact of describing the dynamics in the  $\vec{r}_1, \vec{r}_2$  coordinate system. If we use the coordinate system  $\vec{r}_\pm = (\vec{r}_2 \pm \vec{r}_1)/\sqrt{2}$ , then the Hamiltonian becomes

$$H = -\frac{1}{2}\nabla_+^2 - \frac{1}{2}\nabla_-^2 + 1/(\sqrt{2}r_-) + U(|\vec{r}_+ + \vec{r}_-|/\sqrt{2}) + U(|\vec{r}_+ - \vec{r}_-|/\sqrt{2}). \quad (2)$$

Now the correlation in the dynamics arises from the short-range potentials  $U$ . In the final state, these potentials are effectively zero since both  $r_1$  and  $r_2$  are large, but the initial state is highly correlated in this coordinate system. Fortunately, there is no rule that forces the use of the same coordinate system for both the initial and final state; choosing the same coordinate system is simply a matter of convenience.

The best first order method for calculating the  $T$  matrix involves using an initial state in  $\vec{r}_1, \vec{r}_2$  coordinates and the final state in  $\vec{r}_+, \vec{r}_-$  coordinates. The zeroth order initial state is

$$\psi_i^{(0)} = \frac{1}{\sqrt{2}} \{R_{\ell_b}(r_1)F_{\ell_i}(r_2)[Y_{\ell_b}(\hat{r}_1)Y_{\ell_i}(\hat{r}_2)]_M^L \pm R_{\ell_b}(r_2)F_{\ell_i}(r_1)[Y_{\ell_b}(\hat{r}_2)Y_{\ell_i}(\hat{r}_1)]_M^L\}, \quad (3)$$

where  $R_{\ell_b}(r)Y_{\ell_b}(\hat{r})$  is the wave function for the weakly bound electron,  $F_{\ell_i}(r)Y_{\ell_i}(\hat{r})$  is the wave function for the incident electron, and the two electrons are coupled to total angular momentum,  $L$ , with the  $z$  component being  $M$ . The incident electron's wave function is the solution of a one particle Hamiltonian with a potential  $\tilde{U}(r)$  which has the form  $1/r$  as  $r \rightarrow \infty$ ; the proper choice for  $\tilde{U}(r)$  for smaller  $r$  is discussed below. The incident continuum wave is normalized per unit energy. The  $+$  ( $-$ ) in Eq. (4) is for the singlet (triplet) wave function.

The wave function for the weakly bound electron is extremely difficult to obtain. The procedure adopted here is very similar to that used in Ref. [14]. A short-range, nonlocal potential generates the orbital with the strength and the range of the potential chosen so that the binding energy and asymptotic form of the wave function match that of more accurate multielectron calculations. For  $H^-$  the asymptotic normalization and binding energy was chosen to match that of Ref. [15], while the asymptotic normalization and binding energy for  $B^-$  was chosen to match that of Ref. [16].

The final state wave function is

$$\psi_f = \sqrt{\frac{2k_+}{\pi}} j_{\ell_+}(k_+r_+)f_{\ell_-}(r_-)[Y_{\ell_+}(\hat{r}_+)Y_{\ell_-}(\hat{r}_-)]_M^L, \quad (4)$$

where  $E_+ = k^2 + /2$ ,  $j_{\ell}$  is the spherical Bessel function, and  $f_{\ell}(r)Y_{\ell}(\hat{r})$  is the solution of the Schrödinger equation for a repulsive Coulomb potential with charge  $1/\sqrt{2}$ . The  $f_{\ell_-}$  and  $\sqrt{2k_+/\pi}j_{\ell_+}$  are normalized per unit energy. The triplet wave function has  $\ell_-$  equal to an odd integer while  $\ell_+$  is an even integer for the singlet wave function. The energies for the initial state are the energy of the weakly bound electron,  $E_b$ , and the energy of the incident electron,  $E_i$ . The energies for the final state are the energy in the  $+$  degrees of freedom,  $E_+$ , and the energy in the  $-$  degrees of freedom,  $E_-$ . Conservation of energy means  $E_{\text{tot}} = E_b + E_i = E_+ + E_-$ , where  $0 \leq E_+ \leq E_{\text{tot}}$ .

The most important parameters needed to calculate the cross section are the  $T$ -matrix elements. If the exact final state wave function is known, the  $T$ -matrix elements are given by

$$T_{i,f} = \pi \int [(E - H)\psi_i^{(0)}]^* \psi_f dV. \quad (5)$$

The form used for  $\tilde{U}(r)$  at small  $r$  is *irrelevant* to the accuracy of the  $T$ -matrix elements if the final state wave function is exact. The final state wave function in Eq. (4) is not exact but is very accurate. Indeed, the total detachment cross section changed by at most 15% if  $\tilde{U}(r)$  was chosen to be  $1/r$  for all  $r$  or if  $\tilde{U}(r)$  was chosen to be a screened potential  $\tilde{U}(r) = [1 - \exp(-2\kappa_b r)]/r + \kappa_b \exp(-2\kappa_b r)$ , with  $\kappa_b = \sqrt{-2E_b}$ .

For a fixed  $E_+$ , the cross section differential in  $E_+$  is

$$\frac{d\sigma}{dE_+} = \frac{2\pi}{E_i} \sum_{\ell_i, \ell_+, \ell_-} \frac{(2L+1)(2S+1)}{(2\ell_b+1)4} |T_{\ell_b, \ell_i, \ell_+, \ell_-}^{LS}|^2. \quad (6)$$

The total cross section is obtained by integrating the differential cross section over  $E_+$  from 0 to  $E_{\text{tot}}$ . The  $T$ -matrix elements are only nonzero when the  $L, M$  are the same for the initial and final states. This can be derived from the fact that  $L_{1x} + L_{2x}$  is the same operator as  $L_{-x} + L_{+x}$  (and similarly for  $y$  and  $z$ ).

The difficulty in using this method rests in the evaluation of the several hundreds of  $T$ -matrix elements for each value of  $E_+$  for a fixed  $E_i$ . The six-dimensional integral may be reduced to a five-dimensional integral for the  $T$ -matrix elements since the  $z$  component of the total angular momentum is the same for initial and final states. The five coordinates integrated over are  $r_1, r_2, \cos \theta_1, \cos \theta_2$ , and  $\phi_2 - \phi_1$ . The integration was performed with an unweighted Monte Carlo technique using Sobel's sequence of quasirandom numbers in five dimensions [17]. The only possible spikiness in the integrand is near points  $r_- = 0$ . Since  $f_{\ell_-}(r_-) \propto r_-^{\ell_-}$ , the only problem arises when  $\ell_- = 0$ . The divergence at  $r_- = 0$  is integrable so the  $1/r_-$  term in the potential was replaced with  $3/(2\Delta r)$  whenever  $r_- < \Delta r$ , where  $\Delta r < 0.1$ . The range of integration in  $r_1$  and  $r_2$  was such that  $r_1 \leq 6/\sqrt{-2E_b}$  and  $r_2 \leq 20\pi/\sqrt{2E_i}$ . Convergence of the integral with the number of points was surprisingly rapid. Most of the calculations were performed with  $2^{15}$

and  $2^{16}$  points. The total cross section for the two different numbers of points rarely exceeded 2%. Because each of the integrals for the different  $\ell_i$ ,  $\ell_+$ ,  $\ell_-$ , and  $L$  combinations are independent, this problem is ideally suited for a massively parallel machine. For a fixed  $E_i$  and  $E_+$ , all of the different angular momentum combinations were partitioned between 16 processors with the results from the different processors combined as a last step. However, it must be stressed that the surprisingly rapid convergence of the integrals would allow calculation on a workstation or personal computer. The details of the integrand evaluation will be presented elsewhere.

One last point of physics is used in the practical calculation of the total cross section. To accelerate the convergence of the cross section with the maximum value of  $\ell_i$ , a different approximation is utilized to obtain the contribution to the cross section for  $\ell_i > \ell_{i,\max}$ . In this procedure, we note that  $\ell_{i,\max}$  is so large that the incident electron is always well outside of the negative ion's charge cloud. Very little energy and angular momentum is given to the negative ion. For the final state in this situation, we use a free electron wave for the detached electron and a repulsive Coulomb wave for the scattered electron. Exchange is negligibly small for  $\ell_i > \ell_{i,\max}$ .

The results of the calculations are compared to recent experimental results for  $e^- + \text{H}^- \rightarrow \text{H} + 2e^-$  [5,6] in Fig. 1 and  $e^- + \text{B}^- \rightarrow \text{B} + 2e^-$  [8] in Fig. 2. The results appear to be converged with respect to the number of points used in the five-dimension integration and with respect to maximum angular momentum. The experimental energies have been increased by 0.1 eV to bring them into agreement with the calculation. The uncertainty in the overall experimental normalization of the  $\text{H}^-$  ( $\text{B}^-$ ) cross

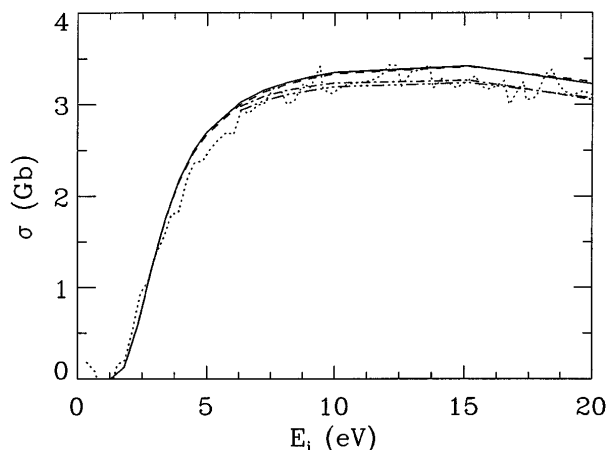


FIG. 1. Total electron impact detachment cross section of  $\text{H}^-$  versus the energy of the incident electron. The experimental points from Ref. [6] are plotted as the dotted line. The various calculations are as follows: solid line ( $2^{16}$  points,  $\ell_{i,\max} = 10$ ); short-dashed line ( $2^{15}$  points,  $\ell_{i,\max} = 10$ ); dot-dashed line ( $2^{16}$  points,  $\ell_{i,\max} = 15$ ); and dot-dot-dot-dashed line ( $2^{15}$  points,  $\ell_{i,\max} = 15$ ).

section is 25% (30%). The experimental  $\text{H}^-$  ( $\text{B}^-$ ) cross section has been multiplied by 1.07 (1.03). Both factors are well within the experimental uncertainty.

While the good agreement between experiment and calculation validates the approximations discussed above, internal evidence also points to the accuracy of the approximations. The main evidence is the insensitivity of the total cross section to the potential used to generate the incident continuum wave. At energies below  $E_i \sim -2E_b$ , the difference between the cross section when using a pure  $1/r$  and screened  $1/r$  potential for  $\tilde{U}(r)$  was completely negligible. The largest difference was  $<15\%$  at energies  $\sim(4-10)$  times the detachment threshold energy. Another check was that the specific form of the short-range potential,  $U(r)$ , had no effect as long as the bound state energy and asymptotic normalization of the negative ion orbital was correct. The error due to the finite number of points in the numerical integration was less than 3%. The error due to truncation of the ranges of angular momenta is estimated to be less than 10%. The estimated total error for the calculation is less than 20%.

The cross section differential in energy gives valuable insight into the dynamics that controls the detachment process. In Fig. 3, the scaled differential cross section,  $S \equiv (d\sigma/dE_+)E_{\text{tot}}/\sigma$ , is plotted for  $\text{H}^-$  versus the scaled energy  $\epsilon_+ = E_+/E_{\text{tot}}$ . These scaling factors were chosen so the range of  $\epsilon_+$  is independent of  $E_i$  and  $\int S(\epsilon_+)d\epsilon_+ = 1$ . The incident energies are 1.5 eV for the solid line, 5 eV for the dotted line, and 10 eV for the dashed line. At low incident energy, only a small fraction of the total energy after the detachment is in the  $\vec{r}_+$  degrees of freedom which means most of the available energy is in the  $\vec{r}_-$  degrees of freedom. However, the concentration of energy in the  $\vec{r}_-$  degrees of freedom after the detachment can be obscured when plotting the results in the  $\vec{r}_{1,2}$  coordinates. For  $\epsilon_+ = 0.07$ , the minimum

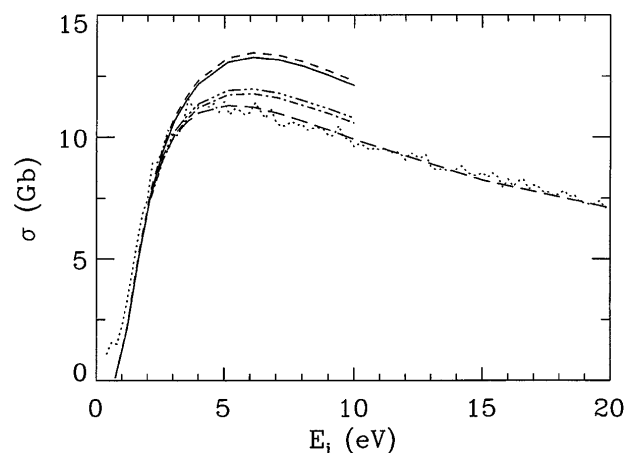


FIG. 2. Same as Fig. 1 but for  $\text{B}^-$  with experimental points from Ref. [8]. The long-dashed line is for  $2^{15}$  points,  $\ell_{i,\max} = 20$ .

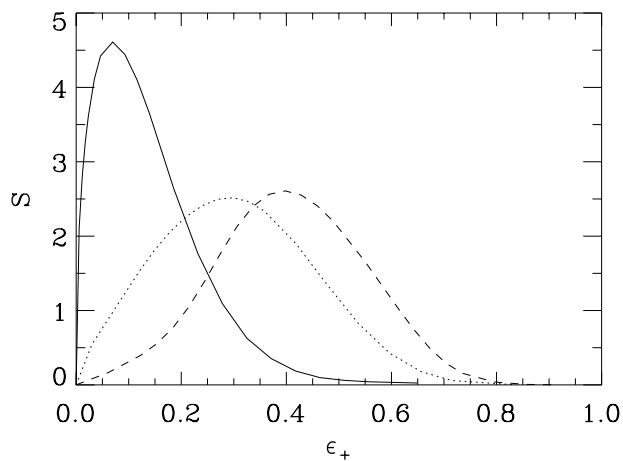


FIG. 3. The scaled differential cross section for  $H^-$  where  $S = (d\sigma/dE_+)E_{\text{tot}}/\sigma$  and  $\epsilon_+ = E_+/E_{\text{tot}}$ . Solid line is for  $E_i = 1.5$  eV; the dotted line is for  $E_i = 5$  eV; and the dashed line is for  $E_i = 10$  eV.

angle between the two outgoing electrons must be larger than  $150^\circ$ , and the ratio of the two momenta must be between 0.57 and 1.76. At the higher incident energies, the  $E_-$  and  $E_+$  do become more nearly equal because the incident electron retains most of the energy, giving one fast electron and one slow electron in the double continuum.

The behavior exemplified in Fig. 3 is a consequence of the  $T$ -matrix element. At low energies, the  $1/r_-$  repulsive potential has a larger effect than the repulsive centrifugal potential which means the matrix element is larger when most of the energy is  $E_-$ . This behavior suggests that the detachment process mainly occurs when the incident electron is at its minimum distance from the weakly bound electron; this is the point of minimum kinetic energy. All of the potential energy is in the  $1/\sqrt{2}r_-$  term and this potential energy will mainly be converted into kinetic energy in the  $\vec{r}_-$  coordinate.

Another interesting feature that arises is the scaling properties of the cross section. For a given angular momentum of the weakly bound electron, if  $\tilde{U}(r) = 1/r$  is chosen to calculate  $F_{\ell_i}(r)$ , then the total cross section  $\sigma(E) \approx N_b^2 \bar{\sigma}(E/|E_b|)/E_b^2$ , where  $\bar{\sigma}$  depends only on the angular momentum of the weakly bound electron and on the scaled energy  $E/|E_b|$  (the factor  $N_b$  is from the asymptotic normalization of  $R_{\ell_b} \sim \sqrt{\kappa_b} N_b \exp(-\kappa_b r)/r$  and becomes roughly independent of  $\kappa_b$  for very weak binding energies). Note that, if this scaling rule holds, the  $e^- + B^- \rightarrow B + 2e^-$  cross section may be used to estimate that the  $e^- + Ca^- \rightarrow Ca + 2e^-$  cross section will peak at  $\sim 1.4$  Tb near 0.5 eV, the  $e^- + Sr^- \rightarrow Sr + 2e^-$  cross section will peak at  $\sim 300$  Gb near 1 eV,

and the  $e^- + Ba^- \rightarrow Ba + 2e^-$  cross section will peak at  $\sim 40$  Gb near 2.5 eV.

In conclusion, an accurate method for calculating the electron impact detachment cross section for weakly bound negative ions has been implemented. This method involves expressing the initial state as functions of  $\vec{r}_1$  and  $\vec{r}_2$  while expressing the final state as a separable function of  $\vec{r}_\pm = (\vec{r}_2 \pm \vec{r}_1)/\sqrt{2}$ . The differential cross section has given some insight into the interesting dynamics governing the detachment process. This method also suggests a scaling rule for the cross section which gives a peak cross section for  $e^- + Ca^- \rightarrow Ca + 2e^-$  at  $\sim 1-2$  Tb. In future papers, the details of the calculation will be presented along with a detailed investigation of the total and differential cross sections in the threshold region.

This work was supported by the DOE. Computations were performed at the National Energy Research Supercomputer Center in Berkeley, California. I thank L. H. Andersen for providing data before publication and C. Froese-Fischer for providing the  $B^-$  orbitals from Ref. [16] in numerical form. I acknowledge discussions of this problem with M. S. Pindzola.

- 
- [1] G. Tisone and L. M. Branscomb, Phys. Rev. Lett. **17**, 236 (1966); Phys. Rev. **170**, 169 (1968).
  - [2] D. F. Dance, M. F. A. Harrison, and R. D. Rundel, Proc. R. Soc. London A **299**, 525 (1967).
  - [3] B. Peart, D. S. Walton, and K. T. Dolder, J. Phys. B **3**, 1346 (1970).
  - [4] B. Peart, R. Forrest, and K. T. Dolder, J. Phys. B **12**, L115 (1979); **12**, 847 (1979).
  - [5] L. H. Andersen, D. Mathur, H. T. Schmidt, and L. Vejby-Christensen, Phys. Rev. Lett. **74**, 892 (1995).
  - [6] L. Vejby-Christensen *et al.*, Phys. Rev. A **53**, 2371 (1996).
  - [7] T. Tanabe *et al.*, Phys. Rev. A **54**, 4069 (1996).
  - [8] L. H. Andersen *et al.*, Phys. Rev. A **58**, 2819 (1998).
  - [9] F. Robicheaux, R. P. Wood, and C. H. Greene, Phys. Rev. A **49**, 1866 (1994).
  - [10] M. S. Pindzola, Phys. Rev. A **54**, 3671 (1996).
  - [11] V. N. Ostrovsky and K. Taulbjerg, J. Phys. B **29**, 2573 (1996).
  - [12] A. K. Kazansky and K. Taulbjerg, J. Phys. B **29**, 4465 (1996).
  - [13] J. T. Lin, T. F. Jiang, and C. D. Lin, J. Phys. B **29**, 6175 (1996).
  - [14] T. Ohmura and H. Ohmura, Phys. Rev. **118**, 154 (1960).
  - [15] C. L. Pekeris, Phys. Rev. **126**, 1470 (1962).
  - [16] C. Froese Fischer, A. Ynnerman, and G. Gaigalas, Phys. Rev. A **51**, 4611 (1995).
  - [17] W. H. Press, S. A. Teukolsky, W. T. Vetterling, and B. P. Flannery, *Numerical Recipes* (Cambridge University Press, Cambridge, England, 1992), 2nd ed.